Available online at www.sciencedirect.com
ScienceDirect
Journal of the European Ceramic Society 27 (2007) 1389–1394
www.elsevier.com/locate/jeurceramsoc

Alumina–zirconia layered ceramics fabricated by stacking water processed green ceramic tapes

J. Gurauskis, A.J. Sánchez-Herencia, C. Baudín *

Instituto de Cerámica y Vidrio (CSIC), C/Kelsen 5, 28049 Madrid, Spain

Available online 6 June 2006

Abstract

Lamination of stacked green ceramic tapes is one of the most attractive methods for the production of multilayer ceramics with strong interfaces. In this work the fabrication of high density layered ceramics by joining ceramic green tapes processed from aqueous ceramic slurries is described. Layers with different thickness and compositions in the alumina–zirconia system were combined to obtain layered ceramics with R-curve behaviour. The optimization of the sintering schedule to obtain crack free structures is described. The mechanical behaviour of the laminates, characterized by the indentation strength method, is discussed in terms of that of the constituent layers and the residual stresses developed.

Keywords: Al_2O_3; ZrO_2; Joining; Sintering; Mechanical properties

1. Introduction

Present-day applications of engineering ceramics require improved mechanical performance. One of the approaches to achieve this is to activate rising crack growth resistance (R-curve) by inducing toughening mechanisms.[1] However, as most toughening mechanisms that originate R-curve behaviour are related to the development of residual stresses at the microstructural level, flaw tolerance for large crack sizes is usually associated with low strengths at small-flaw values. As a solution to this tradeoff, ceramic laminates with strong interfaces and external layers in compression are proposed. The processing of these laminated ceramic structures requires understanding of the nature of the residual stresses in order to obtain defect free structures with operative reinforcing layers.[2–5]

One of the most versatile ceramic systems is Al_2O_3–ZrO_2.[1,3,6–9] In this system, composite layers with different compositions can be combined to give rise the desired residual stresses in the layers for macro-structural scale reinforcement. In addition, the presence of ZrO_2 might originate reinforcing mechanisms,[10,11] which operate at the microstructural level.

In this work Al_2O_3 tapes with 5 and 40 vol.% additions of t-ZrO_2 (Y-TZP) were employed to fabricate laminate ceramic composites by stacking water processed green ceramic tapes.[12,13] The structural distribution of the layers was designed to develop different levels of compressive residual stresses in the external layers. In these laminates the micro-structural and macro-structural reinforcement mechanisms would be activated. The analysis of dilatometry data was done to control the formation of processing defects and to evaluate the level of residual stresses.

In order to assess the R-curve behaviour of the obtained materials during fracture, the indentation strength method has been used. Materials without R-curve behaviour display indentation load $P^{-1/3}$ versus strength dependence.[14,15] A deviation from that ideal $P^{-1/3}$ dependence towards a plateau strength level indicates that R-curve mechanism is operative. The effect of composition of laminated structures on indentation strength behaviour (using loads between 10 and 400 N) is discussed in terms of the associated residual stresses.

2. Experimental

Tapes for the production of the multilayer structures were cast from stable slurries of high purity α-Al_2O_3 and Y-TZP powders in deionised water as dispersing media. The starting powders of α-Al_2O_3 (Condea HPA 0.5, USA), with mean particle size of 0.35 μm and specific surface area of 9.5 m^2/g, and a t-ZrO_2 stabilized with 3 mol.% Y_2O_3 (TZ3YS, TOSOH, Japan), with a mean particle size of 0.4 μm and a specific surface area of 6.7 m^2/g, were used. Two compositions, 95 vol.% of α-Al_2O_3

* Corresponding author. Tel.: +34 917 355 840; fax: +34 917 355 843.
E-mail address: cbaudin@icv.csic.es (C. Baudín).

0955-2219/$ – see front matter © 2006 Elsevier Ltd. All rights reserved.
doi:10.1016/j.jeurceramsoc.2006.04.081

Table 1
Basic composition and solid loading of the tapes fabricated

Tapes	Composition (vol.%)		Solid content (vol.%)	Green density (th.%)
	α-Al_2O_3	Y-TZP		
A-5	95	5	50	$59.1^{\pm0.1}$
A-5(I)			47	$56.2^{\pm0.1}$
A-40	60	40	47	$53.5^{\pm0.1}$
A-40(1)			50	$55.1^{\pm0.1}$

with 5 vol.% of t-ZrO_2 (named A-5) and 60 vol.% of α-Al_2O_3 with 40 vol.% of t-ZrO_2 (named A-40) were selected. For each composition, two slurries with different solid content (Table 1) were prepared in order to obtain the tapes with different green density values. Slurry stabilisation was performed with 0.8 wt.% (referred to solid content) polyelectrolyte Dolapix CE 64 and 5 wt.% of binder DM 765 (referred to solid content) was added to suspension to obtain sufficient elasticity of green tapes. After casting, the green ceramic tapes were dried at room temperature for 24 h and subsequently at 60 °C for 48 h. The final thickness of the green tapes obtained varied between ≈480 and 520 μm.

Dried and round shaped ($\emptyset_{green}$ = 60 mm) tapes were submerged in water for 1 min, coated with the gluing agent (water suspension of 5 wt.% of DM765) and stacked to obtain the laminated pieces after cold uniaxial pressing of 18 MPa. Full experimental details of the green processing, gluing agent selection and pressing procedure are given elsewhere.[12,13] Monolithic pieces were formed by piling seven tapes of the same compositions while laminates were formed by piling seven tapes of different compositions.

Two different distributions of tapes were selected in a way to obtain two different symmetrical laminated architectures with external A-5 layers. In one of them (L1) four A-5 layers were alternated with three A-40 layers of the same thickness (≈500 μm). In the other (L2) three A-5 layers (≈500 μm) were alternated with two A40 layers of double thickness (≈1000 μm).

Binder burn out (1 °C/min up to 600 °C with a dwell time of 30 min) and sintering (2 °C/min up to 1550 °C with a dwell time of 2 h) were performed in a single thermal treatment.

The apparent densities of the green and sintered monolithic pieces were determined by the Archimedes method in mercury and water, respectively. Relative densities were calculated as % of the calculated theoretical density of the studied composition, using 3.99 g/cm^3 for α-Al_2O_3 (ASTM 42-1468) and 6.10 g/cm^3 for Y-TZP (ASTM 83-113). Dilatometric curves of green monolithic samples (5 mm × 5 mm × 4 mm) were recorded in a differential dilatometer with alumina support using platinum protection (Setaram, Setsys-16/17, France) and corrected for alumina expansion. The thermal treatment cycle applied to the samples in the dilatometer was identical to the sintering cycle described previously. The heating up cycle was used to control sintering shrinkage and the cooling down cycle and allowed to evaluate the differences between the actual cooling contractions of the monoliths. The samples were placed in dilatometer having the constituent tapes orientated to the normal direction to the sensor. Two monolithic pieces of each composition were sintered without any previous machining in order to determine the elastic properties from the flexural and torsional mode vibrations. The pieces were placed on the support points allowing first and second natural vibrations of the disc and tested by impact ("GrindoSonic MK5", J.W. Lemmens-Electronica N.V., Belgium). The Young's modulus, E, the shear modulus, G, and the Poisson's ratio, ν, were calculated from the values of the frequencies and the dimensions and densities of the samples.

Laminated green pieces were machined into bars (50 mm × 7 mm × 4 mm) and the surfaces were smoothed with sandpaper before sintering. Polished cross-sections of sintered materials were examined by optical (Carl-Zeiss H-P1, Germany) and by scanning electron (Zeiss DSM-950, Germany) microscopy for interface union defects and for tunnel type defects in the case of symmetrical laminate structures.

The sintered bars were ground to obtain the test samples with final geometry (40 mm × 4 mm × 3 mm). After grinding, the laminate structures had symmetrical distribution of the layers, giving final thickness of ≈420 μm for every constituent layer in laminate L1 and in the case of laminate L2 final thicknesses of ≈420 and ≈840 μm for A-5 and A-40 layers, respectively.

Four-point bending tests were carried out on non-indented and indented samples using universal testing machine (Microtest, Spain) with inner and outer spans of 15 and 30 mm, respectively. The bending load was applied at a constant crosshead speed of 0.05 mm/min. The surface of the bars to be in tension during testing was polished successively using 9, 6 and 1 μm diamond paste and the edges were chamfered after the polishing operation.

Three bending tests for each laminated structure were performed on non-indented bars to determine fracture strength values.

For indentation-strength tests, three Vickers indentations, each 2.5 mm apart, were made in the central part of the tensile surface of the beams. Vickers cracks were made with the normal orientation to the major axis of the beam. The indentations were performed in controlled displacement mode at 0.01 mm/s up to maximum load (10–400 N) with a holding time of 10 s. The indentation imprints were measured within 15 min using optical microscopy. One test was performed at each maximum load level. All fractured samples were examined with an optical microscope to determine whether the fracture proceeded from the indentation. The rising crack growth behaviour (R-curve) was characterized using post-indentation strength–indentation load relation[14,16] using the best-fit curves of the function:

$$\sigma_f = \alpha P^{-\beta} \quad (1)$$

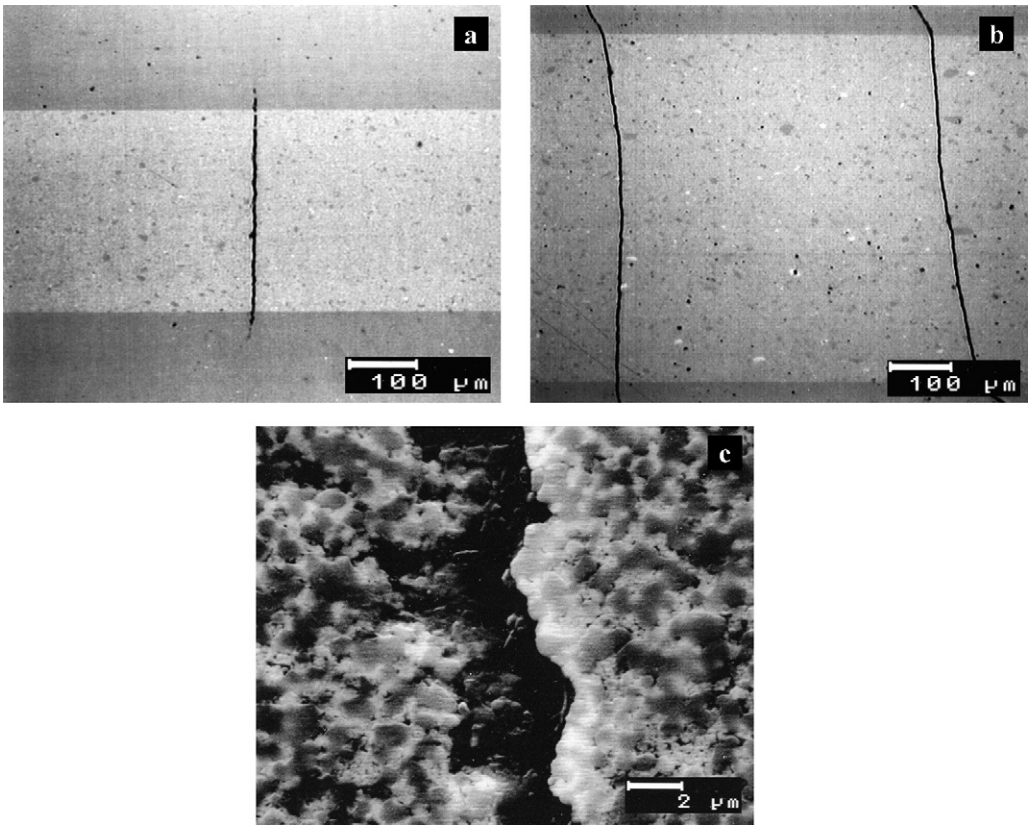

Fig. 1. Transversal cracking observed in symmetrical laminates. (a) Defect pattern in L1 system. (b) Defect pattern in L2 system. (c) Detail of the defect shown in (a).

where, σ_f is the post-indentation strength, P the indentation load, α and β are coefficients describing R-curve behaviour. The standard deviation values from the best-fit curves were used to calculate 95% confidence intervals.

3. Results and discussion

In previous works it was demonstrated that crack free and homogeneous monolithic materials with the compositions A-5 and A-40 starting from seven stacked tapes could be obtained employing the processing route described above.[12,13] Moreover, no residual stresses were observed in those monoliths.[17] Tapes obtained using the optimum colloidal parameters (plasticity, green density, etc.) for each suspension, led to different green densities of 59.1% and 53.5% for A-5 and A-40, respectively. When these tapes were combined to fabricate symmetrical laminates with structures L1 and L2 the cross-sections showed the presence of large transverse cracks though the internal A-40 layers and extending (≈10–30 μm) into the contiguous A-5 layers (Fig. 1a and b). These cracks had large opening displacements (≥20 μm) and smooth crack surfaces with rounded grains (Fig. 1c), suggesting that crack formation took place during sintering. As reported previously,[2,18,19] differential sintering of the layers in ceramics is primary related to density differences. This could be the case of this layered system fabricated using tapes with significantly different green densities. Cai et al.[18] proposed to modify the composition of the solid components of the tapes to reach similar green densities. However, this approach would limit the range of tape compositions to be used. An alternative approach would be to modify the colloidal processing conditions to obtain tapes with compatible green densities. To explore this suggestion, the dilatometric curves recorded during sintering of the monoliths were analyzed (Fig. 2a). Shrinkage started at similar temperatures (≈1050 °C) for both monoliths but around 1150 °C significant differences in shrinkage rate appeared leading to shrinkage differences that increased with temperature. Final shrinkages before the isothermal cycle at 1550 °C were 17% and 22% for A-5 and A-40, respectively. During co-sintering of the layers in the laminated structures this shrinkage difference would lead to the development of densification stresses. According to Cai et al.,[18] these densification stresses cause formation of voids that work as nucleation sites for transversal cracking, as that shown in Fig. 1.

Following these observations, the colloidal processing parameters of the tapes, in particular the suspension solid load, were modified to obtain tapes with similar green densities for both compositions that will be named A-5$^{(I)}$ and A-40$^{(I)}$ (Table 1). The dilatometric curves of monoliths fabricated using these tapes with modified compositions (A-5$^{(I)}$ and A-40$^{(I)}$) are shown in Fig. 2b. Initiation of shrinkage took place at lower temperature for A-5$^{(I)}$ than for A-40$^{(I)}$, and differences in shrinkage levels were maintained up to 1350 °C. From this temperature, both compositions reached similar shrinkage levels and rates, giving final shrinkage mismatch before the high temperature dwell less than ≈1%. These changes in the sintering kinetics of A-5$^{(I)}$ and A-40$^{(I)}$ monoliths, suggested the compatibility of

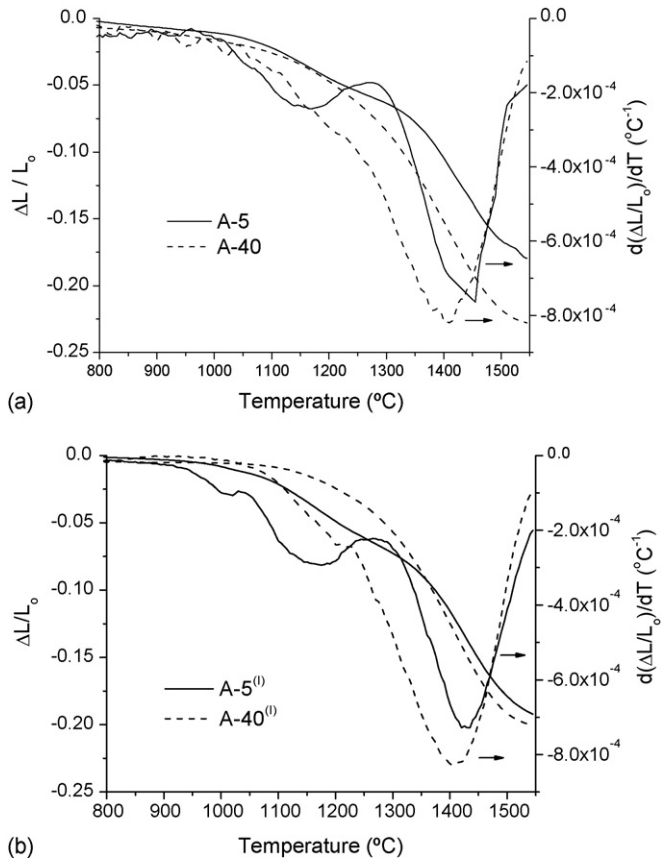

Fig. 2. Dilatometer and sintering kinetics curves for monolithic samples. (a) Samples with different green densities. (b) Samples with adjusted green densities.

tapes with similar green densities for co-sintering in laminated structures. Cross section observation of the sintered laminates fabricated from monoliths with the modified green densities (A-5$^{(I)}$ and A-40$^{(I)}$) showed defect free structures (Fig. 3) with good interface union (Fig. 4) between the constituent tapes.

These results demonstrate that elimination of densifications stresses in the temperature range in which acceleration towards maximum sintering rates of the layers occurs is the most important for these laminated structures. During the initial stage of densification, there were significant differences between sintering levels and rates in A-5$^{(I)}$ and A-40$^{(I)}$ before acceleration occurred (Fig. 2b). Furthermore, the A-40$^{(I)}$ monolith reached the high temperature dwell (1550 °C) almost dense (total shrinkage during dwell time <1%, Fig. 6a), while the A-5$^{(I)}$ monolith experienced significant shrinkage (3%, Fig. 6a) during the isothermal treatment; thus, the layers with composition A-40$^{(I)}$ would be subjected to tensile densification stresses during the final sintering period of the laminates. Nevertheless, none of these features of the sintering behaviour led to cracking of the laminates constituted by these layers for which the temperature ranges for acceleration towards maximum sintering rates were coincident (Fig. 2b). On the contrary, the mentioned temperature ranges for monoliths A-5 and A-40 were significantly different (≈1200–1400 °C and 1350–1450 °C for A-5 and A-40, respectively, Fig. 2a) and transverse cracking took place in the laminates constituted by these tapes (Fig. 1).

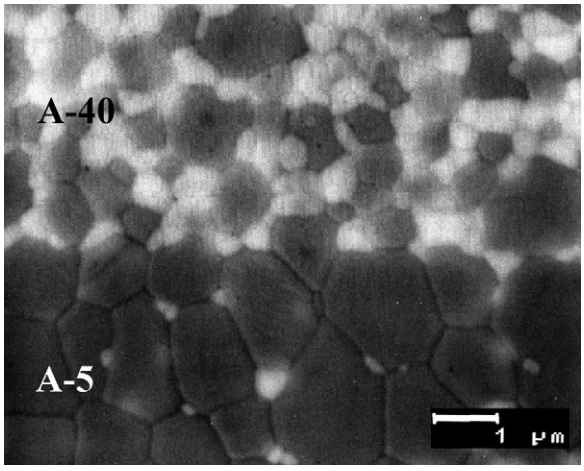

Fig. 4. SEM micrograph, showing interface zone between A-5$^{(I)}$ and A-40$^{(I)}$ tapes. Good and uniform union between layers is observed.

All specimens for testing were fabricated using the optimized tapes A-5$^{(I)}$ and A-40$^{(I)}$ (Table 1). The elastic properties of monolithic samples are given in Table 2.

Fig. 5 plots the indentation strength-indentation load relationships for laminated specimens of systems L1 and L2. Strength values were significantly higher (≈22%) for L2 than for L1 through the whole range of indentation loads, which shows that

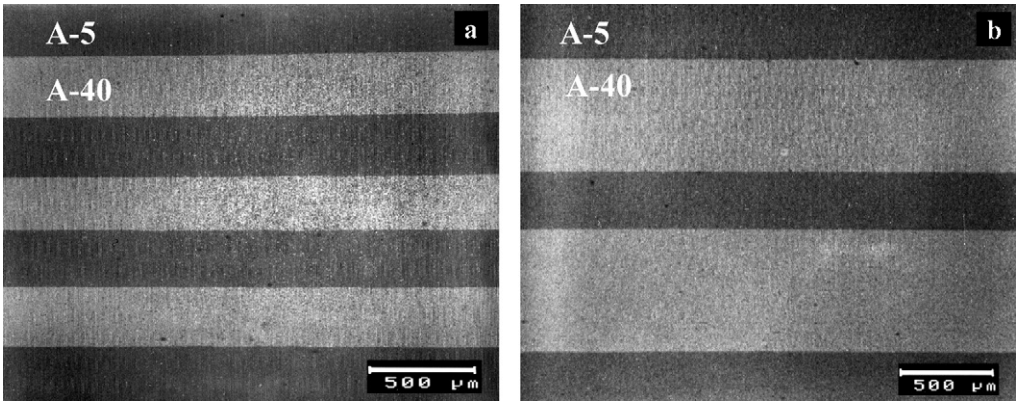

Fig. 3. SEM micrographs at the polished cross-section showing the structure of symmetrical laminates. (a) Laminate L1. (b) Laminate L2.

Table 2
Material properties determined from monolithic pieces

Monolithic material	$\rho_{sintered}$		Young's modulus (GPa)	Shear modulus (GPa)	Poisson coefficient
	g/cm^3	th.%			
A-5$^{(I)}$	$4.03^{\pm0.02}$	$98.7^{\pm0.1}$	$389^{\pm4}$	$155^{\pm2}$	$0.25^{\pm0.01}$
A-40$^{(I)}$	$4.79^{\pm0.01}$	$99.2^{\pm0.1}$	$309^{\pm2}$	$121^{\pm2}$	$0.26^{\pm0.01}$

the laminate structure increased the strength values. In a previous work, the distribution of residual stresses across the section of L1 specimens was determined by the piezo-spectroscopic technique.[9] Compressive stresses were found to develop in the external alumina layers, smaller at the surface and increasing with depth up to maximum values close to the interface between these layers and the contiguous A-40 layers. Maximum stress values determined at the interior of the specimens were of the same order as those calculated using the simplified model (≈190 MPa) of a symmetric plate constituted by alternate layers of the same thickness having a uniform biaxial distribution of stresses across each layer.[20] Using this approach, the arising residual stresses within A-5 and A-40 composition layers are given by:

$$\sigma_{A\text{-}5} = -\frac{\Delta\varepsilon E'_{A\text{-}5}}{1 + (E'_{A\text{-}5} n_{A\text{-}5} h_{A\text{-}5} / E'_{A\text{-}40} n_{A\text{-}40} h_{A\text{-}40})} \quad (2)$$

$$\sigma_{A\text{-}40} = -\sigma_{A\text{-}5} \frac{n_{A\text{-}5}}{n_{A\text{-}40}} \frac{h_{A\text{-}5}}{h_{A\text{-}40}} \quad (3)$$

where $\Delta\varepsilon$ is the strain mismatch between the layers, $n_{A\text{-}5,\,A\text{-}40}$ and $h_{A\text{-}5,\,A\text{-}40}$ are the number and the thickness of the layers, respectively, and $E'_{A\text{-}5,\,A\text{-}40}$ is the reduced Young's modulus:

$$E'_i = \frac{E_i}{1 - \nu_i} \quad (4)$$

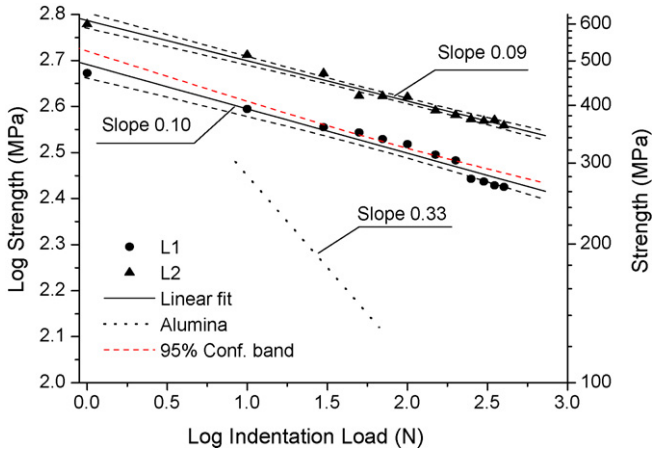

Fig. 5. Logarithm of observed post-indentation strength versus the logarithm of indentation load for the laminate systems studied. The solid lines are linear fit values (Eq. (1)) and the dashed lines are 95% confidence limit. The corresponding fracture strength data versus indentation load scales represented too. As a term of comparison data for fine-grained alumina[14] are also represented.

In order to determine $\Delta\varepsilon$, the cooling part of the sintering cycle from 1200 °C to room temperature was analyzed. This temperature range was chosen because no accommodation of deformation mismatch by diffusional processes occurs in alumina materials at temperatures lower than 1200 °C.[2] In Fig. 6b the analyzed dilatometric curves are plotted. Equal levels of deformation for both compositions at 1200 °C have been assumed because the differences in shrinkage between the layers in the laminates would be accommodated by diffusional processes at high temperatures. From this figure, $\Delta\varepsilon = \varepsilon_{A\text{-}5} - \varepsilon_{A\text{-}40} = 0.9 \times 10^{-6}$, which gives compressive stresses in the A-5$^{(I)}$ layers of −187 and −268 MPa for L1 and L2 structure, respectively. The higher strength values found for L2 as compared to L1 can be explained

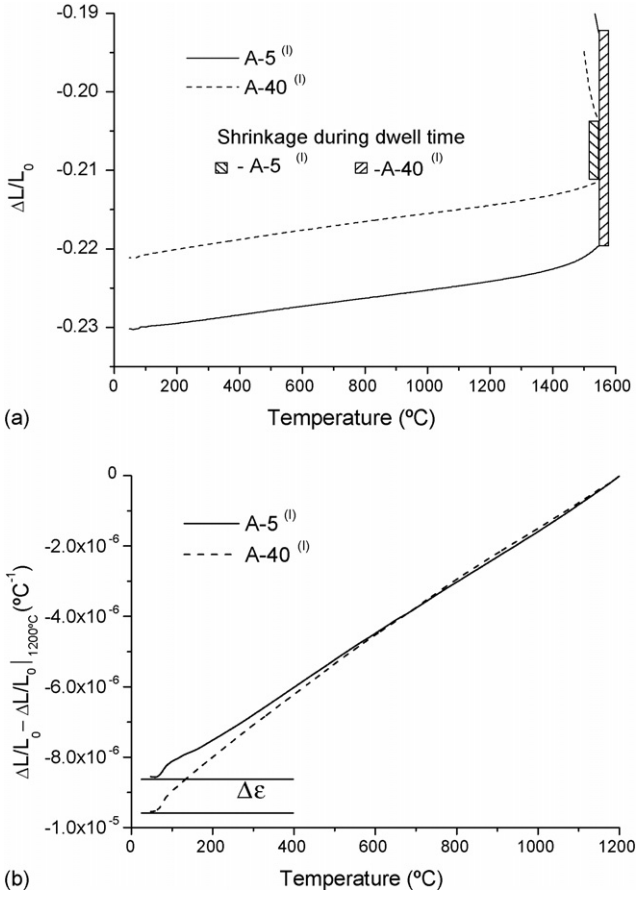

Fig. 6. Dilatometer curves corresponding to A-5$^{(I)}$ and A-40$^{(I)}$ composition samples with similar densities. (a) Data of isothermal cycle (dwell time). (b) Data of cooling down cycle.

by the difference in residual stresses (≈80 MPa) which is of the same order as differences between strength values (≈100 MPa) though the whole range of indentation loads (Fig. 5).

Unlike strength levels, similar β values (Eq. (1)), within the 95% confidence limits, were found for both systems. These values were much lower than the corresponding for fine grained alumina, for which the coefficient β value is 0.33 (indentation load $P^{-1/3}$ versus strength dependence), which reveals similar R-curve behaviour during fracture of both laminated structures, in spite of the level of residual stresses. Taking into account the actual distribution of compressive residual stresses through the external alumina layer, the origin of the observed R-curve behaviour can be envisaged as follows. For small indentation loads (e.g.: 10 N) the cracks associated to the indentations (≈33 μm) are located at the zone of the specimens with low residual stresses. As the indentation load increases, the larger cracks associated are subjected to increasing residual stresses, which leads to increasing apparent toughness. For the maximum load used (400 N), the crack (≈320 μm) has to overcome the high residual stresses found close to the interface (≈420 μm). This process occurs in a similar way for both systems, because the characteristics of the process depend on the thickness of the outer alumina layer and not on the level of residual stresses.

4. Conclusions

Defect free laminated ceramics with strong interfaces and high level of residual stresses can be fabricated from green pieces obtained by stacking water processed tape cast tapes. The matching of density of the constituent tapes is fundamental to allow co-sintering of the different layers.

The strength levels obtained with a particular laminated structure are determined by the actual values of the residual stresses. The relationship between the crack size and its resistance to grow is determined by the distribution of these stresses through the external layer.

Acknowledgments

This work was supported by the projects CICYT MAT 2003-00836 and CAM GR MAT07072004 (Spain).

Work supported in part by the European Community's Human Potential Programme under contract HPRN-CT-2002-00203 [SICMAC].

Jonas Gurauskis acknowledges the financial support provided through the European Community's Human Potential Programme under contract HPRN-CT-2002-00203 [SICMAC].

References

1. Russo, C. J., Harmer, M. P., Chan, H. M. and Miller, G. A., Design of laminated ceramic composite for improved strength and toughness. *J. Am. Ceram. Soc.*, 1992, **75**(12), 3396–3400.
2. Hillman, C., Suo, Z. G. and Lange, F. F., Cracking of laminates subjected to biaxial tensile stresses. *J. Am. Ceram. Soc.*, 1996, **79**(8), 2127–2133.
3. Sánchez-Herencia, A. J., Gurauskis, J. and Baudín, C., Processing of Al_2O_3/Y-TZP laminates from water-based cast tapes. *Compos. B*, in press [available online April 4, 2006].
4. Green, D. J., Cai, P. Z. and Messing, G. L., Residual stresses in alumina–zirconia laminates. *J. Eur. Ceram. Soc.*, 1999, **19**(13–14), 2511–2517.
5. Rao, M. P., Sanchez-Herencia, A. J., Beltz, G. E., McMeeking, R. M. and Lange, F. F., Laminar ceramics that exhibit a threshold strength. *Science*, 1999, **286**(5437), 102–105.
6. Sanchez-Herencia, A. J., James, L. and Lange, F. F., Bifurcation in alumina plates produced by a phase transformation in central, alumina/zirconia thin layers. *J. Eur. Ceram. Soc.*, 2000, **20**(9), 1297–1300.
7. Chartier, T. and Rouxel, T., Tape-cast alumina–zirconia laminates: processing and mechanical properties. *J. Eur. Ceram. Soc.*, 1997, **17**(2–3), 299–308.
8. Cai, P. Z., Green, D. J. and Messing, G. L., Mechanical characterization of Al_2O_3/ZrO_2 hybrid laminates. *J. Eur. Ceram. Soc.*, 1998, **18**(14), 2025–2034.
9. de Portu, G., Gurauskis, J., Micele, L., Sanchez-Herencia, A. J., Baudin, C. and Pezzotti, G., Piezo-spectroscopic characterization of alumina–zirconia layered composites. *J. Mater. Sci.*, in press [available online April 10, 2006].
10. Claussen, N., Stress-induced transformation of tetragonal ZrO_2 particles in ceramic matrices. *J. Am. Ceram. Soc.*, 1978, **61**(1–2), 85–86.
11. Szutkowska, M., Fracture resistance behavior of alumina–zirconia composites. *J. Mater. Proc. Technol.*, 2004, **153–54**, 868–874.
12. Gurauskis, J., Sanchez-Herencia, A. J. and Baudin, C., Joining green ceramic tapes made from water-based slurries by applying low pressures at ambient temperature. *J. Eur. Ceram. Soc.*, 2005, **25**(15), 3403–3411.
13. Gurauskis, J., Sánchez-Herencia, A. J. and Baudin, C., Al_2O_3/Y-TZP and Y-TZP materials fabricated by stacking layers obtained by aqueous tape casting. *J. Eur. Ceram. Soc.*, 2006, **26**(8), 1489–1496.
14. Chantikul, P., Anstis, G. R., Lawn, B. R. and Marshall, D. B., A critical-evaluation of indentation techniques for measuring fracture-toughness. 2. Strength method. *J. Am. Ceram. Soc.*, 1981, **64**(9), 539–543.
15. Chantikul, P., Bennison, S. J. and Lawn, B. R., Role of grain-size in the strength and R-curve properties of alumina. *J. Am. Ceram. Soc.*, 1990, **73**(8), 2419–2427.
16. Krause, R. F., Rising fracture-toughness from the bending strength of indented alumina beams. *J. Am. Ceram. Soc.*, 1988, **71**(5), 338–343.
17. Ruiz-Hervías, J., Bruno, G., Gurauskis, J., Sánchez-Herencia, A. J. and Baudín, C., Neutron diffraction investigation for possible anisotropy within monolithic Al_2O_3/Y-TZP composites fabricated by stacking together cast tapes. *Scr. Mater.*, 2006, **54**(6), 1133–1137.
18. Cai, P. Z., Green, D. J. and Messing, G. L., Constrained densification of alumina/zirconia hybrid laminates. 1. Experimental observations of processing defects. *J. Am. Ceram. Soc.*, 1997, **80**(8), 1929–1939.
19. Cai, P. Z., Green, D. J. and Messing, G. L., Constrained densification of alumina/zirconia hybrid laminates. 2. Viscoelastic stress computation. *J. Am. Ceram. Soc.*, 1997, **80**(8), 1940–1948.
20. Chartier, T., Merle, D. and Besson, J. L., Laminar ceramic composites. *J. Eur. Ceram. Soc.*, 1995, **15**(2), 101–107.